Contrasting patterns of genetic admixture explain the phylogeographic history of Iberian high mountain populations of midwife toads

Federica Lucati[1,2]*, Alexandre Miró[2], Jaime Bosch[3,4], Jenny Caner[2], Michael Joseph Jowers[5,6], Xavier Rivera[7], David Donaire-Barroso[8], Rui Rebelo[1] and Marc Ventura[2]*

[1] Centre for Ecology, Evolution and Environmental Changes (cE3c), Faculty of Sciences, University of Lisbon, Lisbon, Portugal

[2] Center for Advanced Studies of Blanes (CEAB-CSIC), Blanes, Catalonia, Spain

[3] Museo Nacional de Ciencias Naturales-CSIC, Madrid, Spain

[4] Research Unit of Biodiversity - CSIC/UO/PA, Universidad de Oviedo, Mieres, Spain

[5] Centro de Investigação em Biodiversidade e Recursos Genéticos (CIBIO/InBIO), Universidade do Porto, Campus Agrario De Vairão, Vairão, Portugal

[6] National Institute of Ecology (NIE), Seocheon, Republic of Korea

[7] Catalan Society of Herpetology, Leonardo Da Vinci square 4-6, Barcelona, Catalonia, Spain

[8] Calle Mar Egeo 7, Jerez de la Frontera, Cadiz, Spain

* Corresponding authors

E-mail: federicalucati@hotmail.com (FL)

E-mail: ventura@ceab.csic.es (MV)

Abstract

Multiple Quaternary glacial refugia in the Iberian Peninsula, commonly known as "refugia within refugia", allowed diverging populations to come into contact and admix, potentially boosting substantial mito-nuclear discordances. In this study, we employ a comprehensive set of mitochondrial and nuclear markers to shed light onto the drivers of geographical differentiation in Iberian high mountain populations of the midwife toads *Alytes obstetricans* and *A. almogavarii* from the Pyrenees, Picos de Europa and Guadarrama Mountains. In the three analysed mountain regions, we detected evidence of extensive mito-nuclear discordances and/or admixture between taxa. Clustering analyses identified three major divergent lineages in the Pyrenees (corresponding to the eastern, central and central-western Pyrenees), which possibly recurrently expanded and admixed during the succession of glacial-interglacial periods that characterised the Late Pleistocene, and that currently follow a ring-shaped diversification pattern. On the other hand, populations from the Picos de Europa mountains (NW Iberian Peninsula) showed a mitochondrial affinity to central-western Pyrenean populations and a nuclear affinity to populations from the central Iberian Peninsula, suggesting a likely admixed origin for Picos de Europa populations. Finally, populations from the Guadarrama Mountain Range (central Iberian Peninsula) were depleted of genetic diversity, possibly as a consequence of a recent epidemic of chytridiomycosis. This work highlights the complex evolutionary

history that shaped the current genetic composition of high mountain populations, and underscores the importance of using a multilocus approach to better infer the dynamics of population divergence.

Introduction

Patterns of population structure and genetic divergence within species primarily result from their evolutionary history and contemporary dispersal capability, and these processes are in turn responsible of generating specific phylogeographic signatures [1]. The description of these signatures return valuable information on the mechanisms underlying spatial patterns of contemporary genetic diversity and structure, and this knowledge can ultimately help in the conservation and management of species and populations under global change [2].

Organisms with limited dispersal capacity and a typically allopatric type of speciation, such as many amphibians, generally present complex genetic signals at lineage borders resulting in reticulate patterns [3-5]. A number of mechanisms are involved in the generation of reticulate patterns in phylogeography, among them contact zones, hybridisation and introgression [6]. Such mechanisms, among others, may result in the formation of discordant patterns of variation among genetic markers (i.e. mito-nuclear discordances, e.g. [4, 7, 8]). As a consequence, these

69 discordances represent a powerful source of insights into the evolutionary history of
70 species.

71 Quaternary climatic fluctuations had a major impact on worldwide biotas and
72 organisms, reshaping the distribution of species and modelling their genetic structure
73 [9, 10]. In Europe, it is acknowledged that the Iberian Peninsula has served as one of
74 the most important refugia for temperate species during periods of climatic
75 instability [11]. Growing evidence has revealed that in this region, characterized by a
76 great variety of climatic and ecological conditions, multiple isolated refugia were
77 present, which promoted genetic diversification and ultimately determined complex
78 phylogeographic patterns in a number of taxa (the "refugia within refugia" scenario;
79 [11, 12]). In this context, Iberian mountain ranges played a major role in favouring
80 survival throughout the Pleistocene. The Iberian Peninsula has several mountain
81 ranges that permitted flexibility and survival of populations through altitudinal shifts,
82 allowing for movements up or down the mountains in search of suitable
83 microclimates as the temperatures changed [11, 13]. Nevertheless, there is a lack of
84 knowledge on the phylogeographic history of European species with Iberian
85 distribution to understand the role of glacial refugia throughout the different
86 mountain regions within Iberia [11].

87 The common midwife toad (*Alytes obstetricans*) is a small anuran widely
88 distributed in central and western Europe. It is a common species that inhabits a wide
89 variety of habitats between sea level and 2 400 meters above sea level (m.a.s.l.) in

the Pyrenees [14, 15]. Major threats to the species are related to habitat loss and fragmentation through pollution, commercial and agricultural development, introduction of non-native species, and more recently emergent diseases such as chytridiomycosis, which is caused by the chytrid fungus *Batrachochytrium dendrobatidis* (*Bd*) [14-16]. *Bd* has led to episodes of mass mortality in *A. obstetricans*, which is known to be highly susceptible to the pathogen [16-18]. Furthermore, fatal outbreaks of chytridiomycosis in Iberia were more frequent at higher elevations [19].

Alytes obstetricans represents an excellent biological system to study phylogeographic patterns derived from post-glacial expansion, such as contact zones and hybridisation. The species shows strong genetic subdivisions in the Iberian Peninsula, indicative of past population isolation [20]. Until recently, *A. obstetricans* was defined by six divergent and geographically structured mtDNA haplogroups (named A to F; [20, 21]), delineating as many genetic lineages that probably interbreed in zones of secondary contact (Fig 1). Each of the six mitochondrial lineages corresponded to a unique nuclear microsatellite clade, except for lineage B that harboured two distinct microsatellite clusters [22]. More recently, the subspecies *almogavarii* (mtDNA lineages E-F) was proposed as an incipient species (i.e. *A. almogavarii*; [23]) by RAD-sequencing analysis, and mtDNA lineage E described as a novel subspecies (*A. a. inigoi*) [24].

Fig 1. Geographic location of sampling sites for *Alytes obstetricans*/*almogavarii*. The three analysed mountain regions are circled in white. In the Pyrenees, dashed lines delimit the three geographic sections (eastern, central and western Pyrenees). For population codes and further information on sampling sites see S1 Table. The inset map shows the distribution of the main lineages: orange - ND4 haplogroups E-F (*A. almogavarii*), yellow - ND4 haplogroup B (*A. o. obstetricans*), blue - ND4 haplogroup A (*A. o. pertinax*), red - ND4 haplogroup C (*A. o. boscai*), green - ND4 haplogroup D (*A. o. boscai*), black - unclear (adapted from Dufresnes and Martínez-Solano [23]).

Previous studies revealed a complex scenario of relationships and admixture between lineages of *A. obstetricans*/*almogavarii*, evidencing the existence of contact and hybrid zones at some lineage borders [20, 23, 25, 26]. Yet, there has been little attempt on identifying the causes and consequences of such admixture. Furthermore, none of these studies was specifically focused on high mountains, which are well-known hotspots of genetic diversity and have been shown to play a considerable role in separating well-differentiated intraspecific clades in numerous species (e.g. [4, 27]). Here, we employ a multilocus approach combined with comprehensive sample collection across four of the defined mtDNA genetic lineages to analyse the geographical differentiation in *A. obstetricans*/*almogavarii*, placing

special focus on three high mountain regions in the Iberian Peninsula: Pyrenees, Picos de Europa and Guadarrama Mountain Range. Specifically, we aimed to (1) describe finer-scale geographical patterns of genetic diversity and structure in high mountain populations of *A. obstetricans*/*almogavarii*, compare different scenarios of population divergence and explore the role of glacial refugia; (2) identify putative contact zones and assess patterns of admixture; and (3) better delineate the geographic distribution of major genetic lineages. We also provide deeper analyses on the genetic status of populations that have been hit by a recent chytridiomycosis outbreak. To this end, we combined DNA sequence (mitochondrial and nuclear) and microsatellite data for the first time in an *A. obstetricans*/*almogavarii* study. Thus, herein we provide new insights on the recent evolutionary history and the present processes that have shaped and are currently shaping Iberian populations of *A. obstetricans*/*almogavarii*.

Materials and Methods

Sampling and DNA extraction

Sampling was conducted mainly in the period 2009–2018 across northern and central Iberian Peninsula, as it is known to host most of the genetic diversity of the species [20, 22]. We paid special emphasis on three mountain regions: Pyrenees, Picos de Europa mountains (Cantabrian Mountains, NW Iberian Peninsula) and

Guadarrama Mountain Range (central Iberian Peninsula), although we also took some additional samples from neighbouring lowland localities (Fig 1, Tables 1 and S1). We sampled 51 sites in the Pyrenees (1010–2447 m.a.s.l.), 13 in Picos de Europa (1120–2079 m.a.s.l.), nine in Guadarrama Mountains (1527–1980 m.a.s.l.), and 32 sites in lowland areas (52–992 m.a.s.l.), totalling 890 individuals from 105 sampling sites (Table 1). Lowland populations were grouped according to their geographic proximity to the analysed mountain regions (Table 1). A subset of samples was used in a previous study [18].

Table 1. Genetic diversity parameters as estimated from microsatellites for each analysed mountain region and corresponding lowland areas.

	Alt.	N_{pops}	N	Na	Ar	PAAr	H_O	H_E	N_e	ND4 haps
Eastern Pyrenees	1010-2406	17	144	13.47	5.310	0.780	0.480	0.701	14-51	28(F)
Eastern Pyrenees – lowland	62-948	9	21	8.588	5.310	0.830	0.460	0.691	-	11(F)
Central Pyrenees	1211-2003	9	52	10.82	5.130	0.920	0.401	0.651	68	15(E), 4(B)
Central Pyrenees – lowland	567	1	2	-	-	-	-	-	-	2(E)
Central-western Pyrenees	1043-2447	25	284	14.12	5.240	0.990	0.377	0.708	12-84	61(B)
Central-western Pyrenees – lowland	992	1	1	-	-	-	-	-	-	1(B)
Picos de Europa	1120-2079	13	202	12.71	5.740	1.080	0.595	0.789	19-160	31(B)
Picos de Europa – lowland	464-928	3	3	-	-	-	-	-	-	3(B)
Guadarrama	1527-1980	9	112	7.529	3.940	0.580	0.442	0.613	5-15	25(A)
Guadarrama – lowland	52-830	18	57	14.53	6.580	1.080	0.620	0.805	70	36(A), 2(B)

Alt. – altitudinal range, N_{pops} – number of populations, N – sample size for microsatellites, Na – mean number of alleles, Ar – allelic richness standardized for sample size, PAAr – rarefied private allelic richness standardized for sample size, H_O – observed heterozygosity, H_E – expected heterozygosity, N_e – range of effective population size, ND4 haps – occurrence and code (in parentheses) of mitochondrial ND4 haplogroups identified in each deme.

171 Tissue samples were collected via tail clipping in the case of larvae and toe
172 clipping in the case of adults. Samples were stored in absolute ethanol and
173 maintained at -20 °C. Genomic DNA was extracted using QIAGEN DNeasy Blood &
174 Tissue Kit (Qiagen, Hilden, Germany) according to the manufacturer's protocol, or
175 following the HotSHOT method [28], in a final volume of 100 µl for toe clips and 250
176 µl for tail clips.
177

178 Nuclear and mitochondrial genes sequencing

179 We amplified five gene regions, including four mitochondrial fragments
180 (cytochrome *b* gene – cyt-*b*; 12S rRNA gene – 12S; 16S rRNA gene – 16S; and NADH
181 dehydrogenase subunit 4 gene and adjacent tRNAs – ND4) and one nuclear gene (β-
182 fibrinogen intron 7 – β-fibint7). Details on primers used and amplification conditions
183 are provided in S1 Appendix.
184 Resulting sequences were aligned using the ClustalW algorithm in MEGA 7
185 with default settings [29]. Phasing of the nuclear intron β-fibint7 was performed
186 following Gonçalves et al. [20]. Briefly, we used the program SeqPHASE [30] to format
187 the input files, and the Bayesian algorithm implemented in PHASE 2.1.1 [31, 32] to
188 infer phased haplotypes. PHASE was run three times using default values, to check
189 for consistency of haplotype estimation across runs.
190

Microsatellite screening and estimation of genetic diversity

878 individuals from 102 localities were screened for 17 previously characterised microsatellite loci combined in five multiplexes [21]. Fragments were sized with LIZ-500 size standard and binned using Geneious 11.0.5 [33].

The presence of potential scoring errors, large allele dropout and null alleles was tested using MICRO-CHECKER 2.2.3 [34]. We tested for linkage disequilibrium between loci and for departures from Hardy-Weinberg equilibrium (HWE) in each population and for each locus using GENEPOP 4.2 [35]. The Bonferroni correction was applied to adjust for multiple comparisons ($\alpha = 0.05$; [36]).

Genetic diversity parameters were calculated for populations with ≥ five genotyped individuals and for each analysed mountain region and corresponding lowland areas. Observed (H_O) and expected heterozygosity (H_E) and mean number of alleles (Na) were obtained with GenAlEx 6.5 [37]. Allelic richness (Ar) standardized for sample size and rarefied private allelic richness (PAAr – calculated only at the genetic cluster level) were calculated in HP-RARE 1.1 [38]. We estimated the inbreeding coefficient (F_{IS}) within each population with GENETIX 4.05.2 [39].

Phylogenetic analyses

For ND4, we estimated genealogic relationships among haplotypes using Haploviewer [40]. The optimal nucleotide-substitution model was determined by

jModelTest 2.1.3 [41], under the Akaike Information Criterion (AIC). The phylogeny was estimated with RAxML 7.7.1 [42] using a Maximum Likelihood (ML) approach. The program was run with a gamma model of rate heterogeneity and no invariant sites (GTRGAMMA), applying 1 000 bootstrap replicates. The best tree was selected for haplotype network construction in Haploviewer, based on all sequences retrieved from GenBank and this study. Furthermore, genetic diversity parameters, namely number of haplotypes (H) and polymorphic sites (S), as well as haplotype (Hd) and nucleotide (Π) diversity indices, were estimated for the whole dataset and for each analysed mountain region and corresponding lowland areas using DnaSP 6.11.01 [43].

In order to describe the affinities of the different genetic lineages described in *A. obstetricans*/*almogavarii*, we constructed a species tree with the five partially sequenced genes using the multispecies coalescent approach in *BEAST, as implemented in BEAST 2.6.2 (S1 Fig) [44]. The substitution model for each marker was determined by jModelTest. We set a strict molecular clock model and a Yule speciation prior. The clock and tree models for mtDNA markers were linked. We defined five groups in *A. obstetricans*/*almogavarii*, corresponding to the four main population lineages identified in the haplotype network (A, B, E, F) and further subdividing lineage B into two groups (central-western Pyrenees and Picos de Europa; see Results). Since *BEAST does not take into account the possibility of gene flow between lineages, samples from localities where more than one mtDNA

haplogroup was found were excluded from the analysis [20]. Samples of *A. maurus* were used as outgroup. Two independent MCMC chains were run for 200 million generations each, sampling trees and parameter estimates every 5 000. Tracer 1.6 [45] was used to check for stationarity and convergence of MCMC chains. A maximum clade credibility tree was constructed in TreeAnnotator 2.6.2 and visualized using FigTree 1.4.3 (http://tree.bio.ed.ac.uk/software/figtree), discarding the first 10% generations as burn-in, while the node heights were set to mean heights.

Genetic structure

For microsatellites, population structure was inferred using different approaches (S1 Fig): a) a Discriminant Analysis of Principal Components (DAPC) and a Principal Component Analysis (PCA), using the ADEGENET package 2.1.1 [46] in R 3.5.1 [47]; b) a Bayesian cluster analysis implemented in STRUCTURE 2.3.4 [48]; c) a neighbour-joining (NJ) tree using the program POPTREEW [49]; and d) a spatial-based clustering approach implemented in the R package Tess3R 1.1.0 [50], which incorporates geographic coordinates in estimating sample ancestry coefficients. Details on models and parameters used are outlined in S1 Appendix.

To further explore the genetic differentiation between the defined genetic units, we calculated pairwise F_{ST} for both ND4 and microsatellites. Computations were performed in Arlequin 3.5.2.2 [51] in the case of ND4 and in GenAlEx in the case

of microsatellites, with 1 000 permutations to assess statistical significance. Similarly, to partition genetic variability at different hierarchical levels (among genetic clades, among populations within clades and within populations), we conducted an analysis of molecular variance (AMOVA) as implemented in Arlequin, using 10 000 permutations to assess significance of variance components [52]. To better understand the spatial pattern of population differentiation detected in the Pyrenees (see Results), we correlated genetic distances (F_{ST}) of Pyrenean populations either with the Euclidean distance among populations, and with the geographic distance suggested by PCA analysis, which followed a ring-like pattern around the Pyrenean chain assuming no direct gene flow across the central Pyrenean axis (see e.g. [53] for a similar approach). The analysis was performed in GenAlEx with 1 000 permutations, including only populations with ≥ five genotyped individuals (N = 29).

Effective population size

The sibship assignment method implemented in Colony 2.0.6.5 was used to calculate the effective population size (N_e) of populations with ≥ 15 genotyped individuals (S1 Fig) [54]. This software uses a maximum likelihood method to conduct parentage and sibship inference to estimate N_e and can accommodate null alleles and other genotyping errors. The program was run with the parameters specified in Lucati et al. [55]. During sampling care was taken to minimize the effects of sampling

273 individuals belonging to the same clutch, by collecting samples from several spots
274 within the same sampling site.
275

276 Demographic history

277 The approximate Bayesian computation (ABC) approach, as implemented in
278 the software DIYABC 2.1.0 [56], was used to reconstruct the history of divergence
279 among the genetic lineages identified in *A. obstetricans*/*almogavarii*. Only high
280 mountain populations were included in the analysis, as we were interested in
281 understanding the evolutionary history of the three high mountain areas described
282 above (S1 Fig). We grouped populations into five groups according to their
283 geographic location. We also incorporated the information from previous studies
284 dealing with the phylogenetics and population structure of the different subspecies,
285 which point to a shared origin between populations from the central and eastern
286 Pyrenees (mitochondrial ND4 haplogroups E and F in Gonçalves et al. [20] and
287 microsatellite clusters F1n and F2n in Maia-Carvalho et al. [22]): populations from the
288 Picos de Europa mountains (PEU) and the central-western Pyrenees (CWPY;
289 corresponding to subspecies *A. o. obstetricans*) formed two separate groups,
290 whereas populations from the central Pyrenees (CPY), eastern Pyrenees (EPY;
291 corresponding to the putative incipient species *A. almogavarii*) and Guadarrama
292 Mountains (GUA; corresponding to subspecies *A. o. pertinax*) were subdivided into
293 three groups. We generated five different scenarios (Fig 2a): (1) null model with all

294 groups diverging simultaneously from a common ancestor, except for lineage CPY
295 that originates from EPY; (2) sequential splitting model directly following results from
296 STRUCTURE and DAPC analyses, where on the one hand populations from the
297 Pyrenees, and on the other GUA and PEU populations share a common origin; (3)
298 similar to the second one, but predicts a common origin of PEU and CWPY
299 populations, as suggested by ND4 haplotype network; (4) same as the previous
300 scenario, with a common origin between populations belonging to ND4 haplogroups
301 A and B, as suggested by *BEAST analysis; and (5) where the PEU lineage was created
302 by admixture of CWPY and GUA populations. We performed the computations both
303 combining microsatellites and ND4 data, and separately for microsatellites. Further
304 details on model specifications and run parameters are outlined in S1 Appendix and
305 S2 Table.
306
307 **Fig 2. Phylogeographic scenarios tested in DIYABC and best supported models.** (a)
308 Scenarios tested in DIYABC considering the three analysed high mountain areas. (b)
309 The best supported scenarios, namely number 2 when considering only
310 microsatellites and number 5 when considering both mtDNA (ND4) and microsatellite
311 markers, with the estimated divergence times (t1 – t3) of each split. Population
312 groups were defined on the basis of their geographic distribution and the results
313 from clustering analyses: eastern Pyrenees (EPY, orange), central Pyrenees (CPY,

grey), central-western Pyrenees (CWPY, pink), Picos de Europa mountains (PEU, yellow), and Guadarrama Mountain Range (GUA, blue).

Results

Sequence variation and genetic diversity

The nuclear DNA alignment (β-fibint7) included 20 sequences of 605 bp, while for the mitochondrial dataset we obtained 219 sequences of 654 bp for ND4, 40 sequences of 325 bp for cyt-*b*, 42 sequences of 341 bp for 12S, and 40 sequences of 579 bp for 16S (S1 Table). With regard to ND4, overall haplotype (Hd) and nucleotide (Π) diversities were 0.930 ± 0.008 and 0.020 ± 0.0008, respectively. Across the analysed mountain regions, Guadarrama Mountains showed lower ND4 genetic diversity values (Hd = 0.290 ± 0.109, Π = 0.001 ± 0.0002) compared to the other regions (eastern Pyrenees: Hd = 0.770 ± 0.039, Π = 0.002 ± 0.0003; central Pyrenees: Hd = 0.724 ± 0.101, Π = 0.014 ± 0.003; central-western Pyrenees: Hd = 0.805 ± 0.027, Π = 0.002 ± 0.0002; Picos de Europa: Hd = 0.602 ± 0.091, Π = 0.003 ± 0.001).

For microsatellite loci, we did not find evidence of large allele dropout, stuttering or null allele artefacts. Similarly, no significant linkage disequilibrium or departures from HWE across populations and loci were detected after applying the Bonferroni correction. Observed (H_O) and expected heterozygosity (H_E) ranged from 0.197 to 0.794 and from 0.222 to 0.720, respectively (mean H_O = 0.473, mean H_E =

334 0.530; S1 Table). Mean number of alleles (Na) and allelic richness (Ar) varied from
335 2.059 to 7.824 and from 1.270 to 5.620, respectively (mean Na = 4.440, mean Ar =
336 1.873), and the inbreeding coefficient (F_{IS}) ranged from -0.110 to 0.403 (mean =
337 0.157). Among the analysed mountain regions, Picos de Europa and the eastern
338 Pyrenees were the richest regions in terms of genetic diversity, whereas Guadarrama
339 Mountains was the poorest, with the central and central-western Pyrenees
340 presenting intermediate values (Table 1). With regard to lowland areas, populations
341 located in the Duero and Ebro basins (herein referred to as Guadarrama lowland
342 localities) were the most diverse, while eastern Pyrenean localities were the least
343 diverse.
344

345 ## Phylogenetic analyses

346 From the 219 individuals analysed for the ND4 gene we identified 34
347 haplotypes, of which 22 are newly described (Fig 3, S1 Table). Haplotypes were
348 defined by 61 polymorphic sites, of which 49 were parsimony informative. The
349 majority of newly described haplotypes were found in the Pyrenees (13), whereas
350 only three and one haplotypes were detected in Picos de Europa and Guadarrama
351 Mountains, respectively; the remaining five haplotypes were found in lowland
352 localities. The haplotype network showed that haplotypes clustered into four well-
353 differentiated haplogroups with a strong association with geography (Figs 3 and S2a):
354 haplogroup A included sequences from Guadarrama and corresponding lowland

355 areas (corresponding to populations of *A. o. pertinax*), haplogroup F included
356 sequences from the eastern Pyrenees (corresponding to populations of *A.*
357 *almogavarii*), haplogroup E corresponded to populations from the central Pyrenees
358 (*A. a. inigoi*), and haplogroup B (corresponding to populations of *A. o. obstetricans*)
359 included sequences from the central-western Pyrenees and Picos de Europa. Within
360 haplogroup B, sequences corresponding to central-western Pyrenean populations
361 were clearly separated from those from Picos de Europa. In addition, in four localities
362 we detected the presence of more than one haplogroup (Figs 3 and S2a, S1 Table):
363 haplogroups A and B were found to co-occur in population Fte. Nueva de Bardales
364 (T2), whereas both haplogroups B and E were found in populations Plano de Igüer
365 (PI), Balsa Pertacua (BP) and Ibón de los Asnos (61XR).
366
367 **Fig 3. Haplotype network of ND4 sequences analysed in *Alytes***
368 ***obstetricans/almogavarii*.** Each circle represents a unique haplotype and the circle
369 area is proportional to the number of sequences of a given haplotype. Blue dots
370 correspond to inferred unsampled haplotypes. Sequences depicted in white were
371 retrieved from GenBank. The analysed high mountain regions and corresponding
372 lowland areas are indicated by different colours: eastern Pyrenees (EPY, orange),
373 central Pyrenees (CPY, grey), central-western Pyrenees (CWPY, pink), Picos de Europa
374 mountains (PEU, yellow), and Guadarrama Mountain Range and corresponding
375 lowland areas (GUA, blue).

In order to describe the affinities between the different haplogroups, we built a consensus tree with the five sequenced gene fragments using a multispecies coalescent approach (species tree; *BEAST). The tree placed lineage E at the base of the *A. obstetricans*/*almogavarii* lineages, with lineage A as sister to lineage B. Finally, lineage B split into central-western Pyrenees and Picos de Europa groups (S3 Fig).

Genetic structure and effective population sizes

All the clustering analyses performed on microsatellites recovered congruent results (Figs 4, 5 and S2). Regarding DAPC analysis, the optimum number of clusters was inferred to be 7 (Figs 4c, S2b and S4b). The inferred clusters were consistent with the geographic location of populations. A closer look from K = 2 to K = 7 revealed a spatial hierarchical genetic structure (S4a Fig), with a first split between the central-western Pyrenees and all other populations, and a subsequent subdivision of this second group into central Pyrenees–eastern Pyrenees and Guadarrama and corresponding lowland populations–Picos de Europa. At K = 4, populations from the Guadarrama Mountain Range split from lowland populations located in the Duero and Ebro basins and Picos de Europa Mountains, whereas at K = 5 there was a split between the central and eastern Pyrenees. The following splits occurred within the central-western Pyrenean group. According with DAPC analysis, the PCA grouped populations according to their geographic distribution rather than by described

subspecies (Fig 4d). PC1 separated the Pyrenees from the Picos de Europa and Guadarrama, whereas PC2 distributed Pyrenean populations along the Pyrenean chain and contributed to the separation of the Picos de Europa and Guadarrama. STRUCTURE analysis showed patterns of genetic differentiation similar to those inferred by PCA, and identified K = 2 as the best clustering solution (Figs 4a and S5): the first cluster grouped together all Pyrenean populations and the second cluster included peninsular ones. A smaller peak was detected at K = 7 (Fig 4a, 5 and S5b), in agreement with DAPC-inferred clusters, but segregating populations located in the Duero and Ebro basins from Guadarrama Mountains, while splitting central-western Pyrenean populations into two groups. This partitioning into seven clusters was also supported by results of Tess3R analyses (S6 Fig). Furthermore, a higher level of genetic admixture was detected in lowland populations than in highland populations (Figs 5 and S6). More into detail, lowland *A. o. pertinax* populations generally presented the highest degree of admixture, whereas in the Pyrenees moderate levels of admixture were detected between *A. almogavarii* lineage E and *A. obstetricans* in the west, as well as between the two *A. obstetricans* lineages, but not between the two *A. almogavarii* lineages (Fig 5). In order to describe the segregation history amongst the seven groups identified by STRUCTURE, we built a NJ tree based on net nucleotide distances: the tree started at K = 3 with the separation of Guadarrama and corresponding lowland populations from Picos de Europa and the Pyrenees, then at K = 4 populations from the central and eastern Pyrenees split from central-western

418 Pyrenean populations, whereas the following splits occurred within the different
419 major groups (Fig 4b). We also built a second NJ tree inferred from microsatellite-
420 based D_A distances over all populations that identified five discrete lineages, which
421 match with ND4-inferred lineages, except that populations included in haplogroup B
422 formed two separate groups (S2d and S7 Figs). Nevertheless, the tree suggested that
423 the pairs of lineages central Pyrenees–eastern Pyrenees and Guadarrama–Picos de
424 Europa were more closely related with each other than with the lineage of central-
425 western Pyrenees, which in turn appeared more distant from the rest of the lineages.
426
427 **Fig 4. Results of clustering analyses of *Alytes obstetricans/almogavarii* populations**
428 **based on microsatellite data.** (a) STRUCTURE barplots of membership assignment for K =
429 2 and K = 7. Each individual is represented by a vertical bar corresponding to the
430 assignment probabilities to the K cluster. White lines separate populations and black lines
431 separate clusters. (b) Neighbour-joining tree based on net nucleotide distances among
432 the seven clusters inferred by STRUCTURE. Arrows indicate the sequence of
433 differentiation when K increases. (c) Summary plot from Discriminant Analysis of Principal
434 Components (DAPC) for K = 7 genetic clusters. Dots represent individuals and genetic
435 clusters are shown as inertia ellipses. (d) Plot obtained in the Principal Component
436 Analysis (PCA). Each dot represents one individual. Labels indicate the different genetic
437 clusters: eastern Pyrenees (EPY, orange), central Pyrenees (CPY, grey), central-western

438 Pyrenees (CWPY, pink), Picos de Europa mountains (PEU, yellow), and Guadarrama
439 Mountain Range (GUA, blue).
440
441 **Fig 5. Results of Bayesian clustering analysis (STRUCTURE) for K = 7 microsatellite**
442 **groups for *Alytes obstetricans/almogavarii*.** Sampled populations are represented by
443 pie charts highlighting the population cluster membership obtained in STRUCTURE.
444 The inset map shows the distribution of the main lineages: orange - ND4 haplogroups
445 E-F (*A. almogavarii*), yellow - ND4 haplogroup B (*A. o. obstetricans*), blue - ND4
446 haplogroup A (*A. o. pertinax*), red - ND4 haplogroup C (*A. o. boscai*), green - ND4
447 haplogroup D (*A. o. boscai*), black - unclear (adapted from Dufresnes and Martínez-
448 Solano [23]).
449
450
451 The test of significance of pairwise F_{ST} values between the seven lineages
452 defined by STRUCTURE was significantly different from zero ($P < 0.01$; S3 Table),
453 indicating significant genetic differences. ND4-based pairwise F_{ST} values ranged from
454 0.951 for eastern Pyrenees–Guadarrama Mountains to 0.089 for Guadarrama
455 Mountains–Guadarrama lowlands, whereas microsatellite-based pairwise F_{ST} values
456 ranged from 0.222 for Guadarrama Mountains–central-western Pyrenees to 0.060 for
457 Guadarrama lowlands–Picos de Europa. Accordingly, AMOVA analyses suggested
458 significant structure among the seven genetic lineages ($P < 0.001$; S4 Table). The

proportion of variation attributable to differences among lineages was lower in microsatellites (26.171%) than in ND4 (84.945%), possibly as a result of gene flow and the inability of mtDNA to detect it. Conversely, variation among individuals within populations was low for ND4 (8.736%) and high for microsatellite (56.425%) markers, as expected for polymorphic loci such as microsatellites.

In the Pyrenees, microsatellite genetic differentiation followed a ring-like pattern, being maximal between lineages EPY (orange) and CWPY (pink; at opposite extremities on PCA axis 2, Fig 4c-d), even though they are geographically proximate in the central and eastern Pyrenees. To evaluate this hypothesis of ring-shaped isolation by distance, we correlated genetic distances (F_{ST} obtained from microsatellites) of Pyrenean populations to different types of geographic distance. We obtained a weak isolation by distance pattern between genetic differentiation and Euclidean geographic distance (Mantel's R = 0.185, P = 0.002; Fig 6). In contrast, we detected a strong correlation between genetic differentiation and the geographic distance suggested by PCA analysis (Fig 4c-d), which assumed no direct gene flow across the central Pyrenean axis and thus between the two most genetically differentiated lineages EPY and CWPY (Mantel's R = 0.683, P = 0.001; Fig 6).

Fig 6. Isolation by distance analysis over *Alytes obstetricans/almogavarii* population pairs from the Pyrenees. Isolation by distance was calculated based on (a) Euclidean geographic distance between all pairs of populations (Mantel's R =

480 0.185, P = 0.002) and (b) corrected geographic distance as suggested by PCA analysis,
481 i.e. following a ring-shaped distribution around the Pyrenean chain (Fig 4; Mantel's R
482 = 0.683, P = 0.001).
483
484
485 The estimation of effective population sizes conducted in Colony returned, in
486 general, low values (S1 Table). Values ranged from five in the population Laguna de
487 Pájaros (LP) to 160 breeding individuals in the population Lago Ercina (ERC), with a
488 mean N_e of 43. The lowest values were found in populations from the Guadarrama
489 Mountains (N_e range = 5–15), while higher values were found in the Pyrenees
490 (eastern Pyrenees: 14–51, central Pyrenees: 68, central-western Pyrenees: 12–84)
491 and Picos de Europa (19–160).
492

493 Demographic history

494 DIYABC analyses suggested highest support for two different but compatible
495 scenarios of population divergence depending on the genetic markers used (i.e.
496 scenario 2 when using only microsatellites and scenario 5 when combining
497 microsatellites and ND4; Fig 2b, S5 Table). Both scenarios had non-overlapping 95%
498 confidence intervals and type I and II errors for the best supported models were low
499 (S5 Table), indicating high confidence in scenario choice. Model checking confirmed
500 that the best supported scenarios provided a good fit to the observed data (data not

shown). Furthermore, the mean mutation rate estimated for ND4 was found to be an order of magnitude higher than the literature value (1.96×10^{-7} substitutions/site/year; S6 Table), but still much lower than that estimated for microsatellites (ranging from 1.28×10^{-4} to 3.89×10^{-4} and from 4.59×10^{-5} to 3.31×10^{-4} for analyses conducted using only microsatellites and including both ND4 and microsatellite markers, respectively).

The analysis focused on microsatellites indicated that scenario 2 (the sequential splitting model based on results from clustering analyses) was the best supported model (Fig 2b, S5 Table). According to this scenario, the first split led to the separation of Pyrenean populations from peninsular ones. During the second split there was the divergence of, on the one hand, central-western and central-eastern Pyrenean populations, and on the other Picos de Europa and Guadarrama populations. Finally, populations from the central Pyrenees originated from eastern Pyrenean populations during the third split. The first split occurred 56 000–28 000 years ago, and the second and third splits 36 800–18 400 and 25 200–12 600 years ago, respectively (S6 Table). The analysis based on the combination of microsatellites and ND4, however, suggested that Picos de Europa populations were generated by admixture of populations from the central-western Pyrenees and Guadarrama (scenario 5; Fig 2b, S5 Table). Results indicated that the first split occurred 76 200–38 100 years ago, the second split 52 800–26 400 years ago and the admixture event 41 400–20 700 years ago (S6 Table).

Discussion

The Iberian Peninsula is an extraordinary model system to assess the multiple historical vicariance events of species, the so called “refugia within refugia” model, where mountain ranges have had a significant role [11, 12]. Such processes are influenced by climatic and topographic conditions as well as through biological processes between populations, which in turn reflect different and contrasting time scales, historical and contemporary. To unravel such complex scenarios, a multilocus approach is expected to reveal contrasting, often discordant findings that underline intricate evolutionary processes [57]. Several recent studies targeting the Iberian Peninsula and the Mediterranean biodiversity hotspot have focused on the processes of niche divergence and admixture following secondary contact (e.g. Chamorro et al. [58] and Martínez-Freiría et al. [59] with Mediterranean vipers, Antunes et al. [60] with the fire salamander *Salamandra salamandra*, and Dufresnes et al. [61] with *Discoglossus* and *Pelodites* frogs), highlighting the role of these areas as centres of diversification and speciation. The results of the present study revealed a strong association of the defined genetic lineages with geography by using a multilocus analysis of genetic divergence in Iberian high mountain populations of *A. obstetricans*/*almogavarii*. Furthermore, high mountain populations showed higher levels of genetic distinctiveness than lowland populations (Fig 5), suggesting that

542 mountains may have driven population differentiation through long-term geographic
543 isolation, with lowlands more likely to be dispersal corridors for *A.*
544 *obstetricans*/*almogavarii,* as it has been described for other species (see e.g. [62,
545 63]).
546

547 The role of high mountains in genetic differentiation and
548 glacial refugia

549 This study describes the presence of seven different nuclear microsatellite
550 clusters, that are likely a result of recent microrefugial areas within the Pyrenees (Fig
551 5). Most of the recovered genetic structure was within Pyrenean populations, which
552 in turn were genetically more related to each other than with the other two high
553 mountain areas. Putative episodes of admixture within *A. obstetricans*/*almogavarii* in
554 the Pyrenees were suggested by previous phylogenetic analyses [3]. Following the
555 splits between major population lineages in *A. obstetricans*/*almogavarii*, which date
556 back to the Early Pleistocene (starting from 2.5 Mya; [20]), there have been several
557 glacial-interglacial episodes that likely provided opportunities for diverging taxa to
558 come into contact and interbreed following range shifts tracking the climatic
559 fluctuations [12, 64]. Our findings show that Pyrenean high mountain populations
560 have gone through relatively recent events of admixture, likely favoured by the
561 different glacial-interglacial episodes that characterised the Late Pleistocene.

562 Specifically, according to ABC analyses, the two lineages ascribed to *A. almogavarii*
563 (E-F, central and eastern Pyrenees), together with some populations of *A. o.*
564 *obstetricans* (central-western Pyrenean group) seem to have undergone a certain
565 degree of contact and admixture until divergence took place ~36 800–12 600 years
566 ago (Fig 2b). Despite the selected model, which proposes two independent admixture
567 events between the three lineages, the highly overlapping dates together with the
568 significant ring-shaped isolation by distance pattern (Fig 6; see below) suggest that
569 one single admixture event might have occurred within one main glacial refugia
570 where the three lineages coincided. In addition, contemporary signs of connectivity
571 between the two species were detected at lineage borders, as indicated by the
572 occurrence of a contact zone between ND4 lineage E and *A. o. obstetricans* in the
573 west (Figs 3, 5 and S2). Similarly, signs of admixture and extensive gene flow between
574 *A. o. obstetricans* and *A. almogavarii* in the western Pyrenees were previously
575 pointed out by allozyme markers [25, 26]. In contrast, in the central and eastern
576 Pyrenees no signs of connectivity were detected between ND4 lineage F and either
577 lineage E or *A. o. obstetricans*. This scenario of different contact zones telling
578 different stories is exemplified in ring species, i.e. a system formed by a region of
579 interconnected populations with both ends of the ring coming into contact without
580 apparent admixture [65, 66]. In the Pyrenees, the spatial distribution of the *A.*
581 *obstetricans* complex seems to fit with a postglacial colonisation pattern similar to
582 what has been described in ring diversification, where taxa at the western part of the

583 ring likely interbreed and those at the eastern side apparently don't, displaying a
584 continuum from slightly divergent neighbouring populations to substantially
585 reproductively isolated taxa (Figs 4d, 5 and 6). Ring diversifications represent cases of
586 population divergence around a geographical barrier in a ring-like manner [67] that
587 can result in cases of speciation in action (i.e. ring species) and have been cited as
588 evidence of evolution [68], with some of the most well-known cases being identified
589 in herptiles, such as the *Ensatina eschscholtzii* salamander complex [69] and the
590 western fence lizard *Sceloporus occidentalis* [70] in western North America. In light of
591 this, our results are not entirely in line with the distinction of *A. almogavarii* as a
592 different species, yet support a scenario of speciation in action, with lineage F
593 showing evidence for speciation and reproductive isolation [23], and lineage E
594 retaining some degree of connectivity with *A. o. obstetricans*. Nevertheless, we
595 cannot rule out that this pattern may be the result of geographic sampling gaps, and
596 additional surveys across hybrid zones between lineages E-F and *A. o. obstetricans*, as
597 well as further work using resistance distances (i.e. by taking elevation, slope and
598 land cover into account), would be required to fully test the ring species hypothesis.
599 Finally, with regard to the central-western Pyrenean group, the subdivision by
600 microsatellite analyses into two or three different genetic clusters (Figs 4 and S2),
601 points to a scenario of allopatric divergence after the recolonization of the Pyrenees
602 as a result of geographic barriers, with consequent reduction or disruption of gene
603 flow. Alternatively, this differentiation might have happened during one of the abrupt

604 cooling episodes of the Holocene (e.g. the 8 200 year-event; [71]), with consequent
605 isolation in separate glacial refugia. Range isolation and lineage divergence in
606 separate Pyrenean refugia during Pleistocene glacial cycles were also invoked e.g. for
607 the Pyrenean brook newt *Calotriton asper* [55], the ground-dwelling spider
608 *Harpactocrates ravastellus* [72], the rusty-leaved alpenrose *Rhododendron*
609 *ferrugineum* [73] and the snapdragon *Antirrhinum* [74], in line with evidence from a
610 number of other high mountain areas that served as glacial refugia during periods of
611 adverse conditions, such as the Andes, Himalaya and the Southern Alps in New
612 Zealand (see [64] for a review). From a conservation point of view, we suggest that
613 these areas should be treated as separate conservation and management units.

614

615 ## Mito-nuclear discordances

616 The analyses of microsatellites distinguished two highly divergent *A. o.*
617 *obstetricans* lineages, one in the central-western Pyrenees and the other in Picos de
618 Europa (Figs 4 and S2), with the latter being more genetically related to the southern
619 populations (ascribed to *A. o. pertinax*; Figs 4d and S7). In contrast, these two
620 lineages bear the same mtDNA (ND4) haplogroup ascribed to *A. o. obstetricans*
621 (haplogroup B; Figs 3 and S2a). One possible explanation is that the closer genetic
622 affinity of the western and southern area populations rather than to the central-
623 western Pyrenean lineage originated from extensive admixture with *A. o.*

624 *obstetricans* (the central-western Pyrenean group) as the maternal donor and *A. o.*
625 *pertinax* as the paternal donor (Fig 2b). A similar pattern was observed in *S.*
626 *salamandra* [75] and in crustaceans of the genus *Daphnia* [76]. A plausible scenario
627 could be that, during Late Pleistocene glacial periods (as suggested by results from
628 DYABC modelling when combining both microsatellites and mtDNA; Fig 2), some *A. o.*
629 *obstetricans* populations remained confined in isolated refugia where they coincided
630 with *A. o. pertinax* for a sufficient time so that genetic admixture could take place.
631 Similarly, range isolation during Pleistocene climatic fluctuations was suggested for
632 the cryptic *Pelodytes* anuran clade [77, 78], the Cabrera vole *Microtus cabrerae* [79]
633 and the scrub-legume grasshopper *Chorthippus binotatus binotatus* [80], where
634 extant lineages likely diverged in separated refugia within the Iberian Peninsula.
635 Subdivided glacial refugia could have experienced events of admixture during the
636 succession of glacial and interglacial periods, with consequent fusion between
637 refugial lineages [81, 82].

638 Mito-nuclear discordances with evidence for admixture or hybridisation are
639 not uncommon in amphibians (e.g. [4, 8, 60]) and have also been described in a wide
640 range of other animal species from north-central Iberian Peninsula, from arachnids
641 [83] to mammals [84]. Furthermore, the Cantabrian Mountains represent a peculiar
642 biogeographic region and a recognised hotspot of genetic diversity in amphibians,
643 being home to endemic refugial clades in a number of species with broad European
644 distribution [82, 85]. Finally, more recently, the Picos de Europa and *A. o. pertinax*

645 populations may have come into secondary contact and interbred following an
646 expansion phase, creating zones of admixture at lineage borders. Alternatively, the
647 discordance may stem from stochastic processes in the form of genetic drift, and the
648 phylogeographic structure detected in mtDNA (Figs 3 and S3) may have developed as
649 a result of low individual dispersal distances and/or population sizes [86], as
650 evidenced by our results and published literature (e.g. [87]). Further studies and
651 sequencing of more molecular markers are needed to test these hypotheses and
652 enrich our understanding of the phylogeography of *A. obstetricans*.
653

654 Chytridiomycosis and population bottleneck

655 The genetic distinctiveness and limited genetic diversity of populations from
656 the Guadarrama Mountains herein detected (Figs 4 and S2, Table 1) are likely early
657 signs of inbreeding depression induced by an emerging pathogen, i.e. the chytrid
658 fungus *Batrachochytrium dendrobatidis* [88]. It should be noted that our sampling
659 was performed approximately 10 years after an epidemic of the disease
660 chytridiomycosis, which hugely impacted this area in the period 1997–1999, causing
661 several populations to decrease or even disappear [16, 89]. Accordingly, the only
662 sampled population in the affected area that did not show signs of chytridiomycosis
663 was the one presenting the highest genetic diversity (Montes de Valsain, MV; S1
664 Table). Our findings complement those of Albert et al. [18] that detected evidence of
665 low genetic variability and strong population bottleneck in *A. obstetricans* from the

same mountain system. In addition to this, we report on the first estimates of effective population sizes of these populations, which were among the lowest overall (N_e = 5–15; Table 1), raising concern for the long-term persistence of these populations, which are small and isolated. Indeed, the closest neighbouring populations are located more than 50 km away and are known to be small and not genetically related [18, 90]. Furthermore, the Guadarrama Mountains constitute a major barrier to gene flow in amphibians and a key feature shaping population structure and promoting population divergence across taxa [62]. Our results are an example of a disease acting as selective pressure in wild populations by inducing genetic hallmarks of bottlenecks and inbreeding, as it has also been shown in other species such as the black-tailed prairie dog (*Cynomys ludovicianus*), the mountain yellow-legged frog (*Rana muscosa*) and the bobcat (*Lynx rufus*) (reviewed in [91]).

Differences in the evolutionary horizon/resolution between genetic markers

This study confirms previous findings in *A. obstetricans*/*almogavarii* clades [20] with the only difference that our species tree analyses recovered a different basal lineage (S3 Fig), a likely consequence of our limited inference power given that only two loci were used for species tree reconstruction. Results from ABC modelling based on either microsatellites or microsatellites + mtDNA resulted in time estimates

686 highly different from those of the species tree (Fig 2b), suggesting that the two
687 analyses are depicting different evolutionary events. In fact, while the species tree
688 has proven useful to estimate divergence times associated with the formation of
689 species/subspecies, ABC modelling was here employed to gain insights into the
690 colonisation of three high mountain regions in the Iberian Peninsula by the different
691 *A. obstetricans*/*almogavarii* taxa. Microsatellite markers, with their faster mutation
692 rate, are known to perform poorly for the estimation of ancient historical events [57,
693 92]. On the contrary, microsatellites provide substantially better estimations than
694 mtDNA for the most recent dynamics [57]. However, the combination of both
695 markers in our ABC modelling resulted in similar divergence times as those estimated
696 using microsatellites alone. It is thus possible that combining both markers may have
697 biased toward microsatellites and the estimation of recent historical events.
698 We need to stress that DIYABC modelling has some uncertainty. Firstly, this
699 approach is based on scenarios where no gene flow is permitted between
700 populations after they initially diverge. Only single events of admixture between
701 populations are considered, whereas recurrent gene flow due to dispersal cannot be
702 incorporated. However, population structure analyses were used to investigate
703 contemporary gene flow and identify patterns of admixture and contact zones at
704 lineage borders (e.g. Fig 5). Secondly, the tested models do not represent a
705 comprehensive range of all possible scenarios, but are instead based on a selection of
706 contrasting hypotheses that we considered were most likely to reflect our data. We

707 focused our analysis on simple contrasting models aimed at capturing the key
708 demographic events, avoiding overcomplex and redundant models, therefore the
709 selected models should be viewed as a starting point for evolutionary understanding.
710 This approach has proven useful to increase the ability of DIYABC to reveal the
711 correct model, as well as to better estimate the error and accuracy of parameter
712 estimates [93]. On the other hand, it has to be noted that estimates based on
713 mitochondrial data might be unreliable due to the erratic mutation rate of mtDNA
714 and to the fact that mtDNA does not evolve neutrally since transmission of
715 mitochondria is completely linked to maternal inheritance. Indeed, mtDNA-based
716 estimates have been found to mismatch the onset of species divergence in both
717 directions due to the stochasticity of coalescence [94].
718

719 ## Concluding remarks

720 Our multilocus phylogeography across the Iberian Peninsula revealed high
721 genetic structure correlated with geography and a complex pattern of lineage
722 admixture in high mountain populations of *A. obstetricans*/*almogavarii*. Our study
723 evidenced how each analysed mountain region underwent a peculiar
724 phylogeographic history through the Late Pleistocene, which is consistent with the
725 "refugia within refugia" model [11, 12] and confirms previous studies on a number of
726 Iberian amphibian species (e.g. [22, 77, 85, 95, 96]). Results also support the
727 assumption that refugia within refugia may be hotspots of extensive mito-nuclear

728 discordances [82], highlighting the importance of multilocus approaches to infer the
729 dynamics of population divergence. Environmental change in the different mountain
730 systems may have an influence on selection, resulting in an increased divergence
731 among isolated populations, consequently leading to speciation [97]. The phenetic
732 differences between the subspecies of *Alytes* (especially *A. o. pertinax*) may be a
733 further indication of adaptation to some micro-environmental differences such as
734 streams vs still waters (known to influence coloration in *Alytes*, [98]), temperature
735 and solar radiation at different altitudes between the studied mountain systems.
736

737 # Acknowledgements

738 We thank Saioa Fernández-Beaskoetxea, Amparo Mora, Susana Marquínez, Fernando
739 Rivada, René A. Priego, Abel Bermejo and Matthew C. Fisher for field assistance, and
740 Eva Albert, Laura Méndez, Annie Machordom and Andrés Fernández-Loras for
741 laboratory assistance.

References

1. Avise JC. Phylogeography: The history and formation of species. (ELS) iEoLS, editor. Cambridge, MA, USA: Harvard University Press; 2000.
2. Fordham DA, Brook BW, Moritz C, Nogués-Bravo D. Better forecasts of range dynamics using genetic data. Trends in Ecology & Evolution. 2014;29(8):436-43.
3. Gonçalves H, Martínez-Solano I, Ferrand N, García-París M. Conflicting phylogenetic signal of nuclear vs mitochondrial DNA markers in midwife toads (Anura, Discoglossidae, *Alytes*): Deep coalescence or ancestral hybridization? Molecular Phylogenetics and Evolution. 2007;44(1):494-500.
4. Pereira RJ, Martinez-Solano I, Buckley D. Hybridization during altitudinal range shifts: Nuclear introgression leads to extensive cyto-nuclear discordance in the fire salamander. Molecular Ecology. 2016;25(7):1551-65.
5. Denton RD, Kenyon LJ, Greenwald KR, Gibbs HL. Evolutionary basis of mitonuclear discordance between sister species of mole salamanders (*Ambystoma* sp.). Molecular Ecology. 2014;23(11):2811-24.
6. Edwards SV, Potter S, Schmitt CJ, Bragg JG, Moritz C. Reticulation, divergence, and the phylogeography–phylogenetics continuum. Proceedings of the National Academy of Sciences. 2016;113(29):8025-32.
7. Toews DPL, Brelsford A. The biogeography of mitochondrial and nuclear discordance in animals. Molecular Ecology. 2012;21(16):3907-30.
8. Bisconti R, Porretta D, Arduino P, Nascetti G, Canestrelli D. Hybridization and extensive mitochondrial introgression among fire salamanders in peninsular Italy. Scientific Reports. 2018;8(1):1-10.
9. Hewitt GM. The genetic legacy of the Quaternary ice ages. Nature. 2000;405(6789):907-13.
10. Hewitt GM. Genetic consequences of climatic oscillations in the Quaternary. Philosophical Transactions of the Royal Society of London B: Biological Sciences. 2004;359(1442):183-95; discussion 95.
11. Gómez A, Lunt DH. Refugia within refugia: Patterns of phylogeographic concordance in the Iberian Peninsula. In: Weiss S, Ferrand N, editors. Phylogeography of southern European refugia. Amsterdam, Netherlands: Springer; 2007. p. 155-88.
12. Abellán P, Svenning J-C. Refugia within refugia–patterns in endemism and genetic divergence are linked to Late Quaternary climate stability in the Iberian Peninsula. Biological Journal of the Linnean Society. 2014;113(1):13-28.
13. Hewitt GM. Some genetic consequences of ice ages, and their role in divergence and speciation. Biological Journal of the Linnean Society. 1996;58(3):247-76.
14. Bosch J, Beebee T, Schmidt B, Tejedo M, Martinez Solano I, Salvador A, et al. *Alytes obstetricans* (errata version published in 2016). The IUCN Red List of Threatened Species 2009: e.T55268A87541047. doi:10.2305/IUCN.UK.2009.RLTS.T55268A11283700.en. 2009.
15. Miró A, Sabás I, Ventura M. Large negative effect of non-native trout and minnows on Pyrenean lake amphibians. Biological Conservation. 2018;218:144-53.

16. Bosch J, Martínez-Solano I, García-París M. Evidence of a chytrid fungus infection involved in the decline of the common midwife toad (*Alytes obstetricans*) in protected areas of central Spain. Biological Conservation. 2001;97(3):331-7.
17. Tobler U, Schmidt BR. Within- and among-population variation in chytridiomycosis-induced mortality in the toad *Alytes obstetricans*. PLoS One. 2010;5(6):e10927.
18. Albert EM, Fernández-Beaskoetxea S, Godoy JA, Tobler U, Schmidt BR, Bosch J. Genetic management of an amphibian population after a chytridiomycosis outbreak. Conservation Genetics. 2014;16(1):103-11.
19. Walker SF, Bosch J, Gomez V, Garner TW, Cunningham AA, Schmeller DS, et al. Factors driving pathogenicity vs. prevalence of amphibian panzootic chytridiomycosis in Iberia. Ecology Letters. 2010;13(3):372-82.
20. Gonçalves H, Maia-Carvalho B, Sousa-Neves T, Garcia-Paris M, Sequeira F, Ferrand N, et al. Multilocus phylogeography of the common midwife toad, *Alytes obstetricans* (Anura, Alytidae): Contrasting patterns of lineage diversification and genetic structure in the Iberian refugium. Molecular Phylogenetics and Evolution. 2015;93:363-79.
21. Maia-Carvalho B, Gonçalves H, Martínez-Solano I, Gutiérrez-Rodríguez J, Lopes S, Ferrand N, et al. Intraspecific genetic variation in the common midwife toad (*Alytes obstetricans*): Subspecies assignment using mitochondrial and microsatellite markers. Journal of Zoological Systematics and Evolutionary Research. 2014;52(2):170-5.
22. Maia-Carvalho B, Vale CG, Sequeira F, Ferrand N, Martínez-Solano I, Gonçalves H. The roles of allopatric fragmentation and niche divergence in intraspecific lineage diversification in the common midwife toad (*Alytes obstetricans*). Journal of Biogeography. 2018;45(9):2146-58.
23. Dufresnes C, Martínez-Solano Í. Hybrid zone genomics supports candidate species in Iberian *Alytes obstetricans*. Amphibia-Reptilia. 2019;41(1):105-12.
24. Dufresnes C, Hernandez A. Phylogeographic advances in midwife toads (*Alytes*) support the existence of a novel taxon endemic to the Central Pyrenees. Journal of Zoological Systematics Evolutionary Research. 2021;59(8):2170-9.
25. Arntzen JW, Garcia-Paris M. Morphological and allozyme studies of midwife toads (genus *Alytes*), including the description of two new taxa from Spain. Contributions to Zoology. 1995;65(1):5-34.
26. García-París M. Variabilidad genética y distribución geográfica de *Alytes obstetricans almogavarii* en España. Revista Española de Herpetología. 1995;9:133-8.
27. Pöschel J, Heltai B, Graciá E, Quintana MF, Velo-Antón G, Arribas O, et al. Complex hybridization patterns in European pond turtles (*Emys orbicularis*) in the Pyrenean Region. Scientific Reports. 2018;8(1):1-13.
28. Montero-Pau J, Gómez A, Muñoz J. Application of an inexpensive and high-throughput genomic DNA extraction method for the molecular ecology of zooplanktonic diapausing eggs. Limnology and Oceanography: Methods. 2008;6(6):218-22.
29. Kumar S, Stecher G, Tamura K. MEGA7: Molecular Evolutionary Genetics Analysis version 7.0 for bigger datasets. Molecular Biology and Evolution. 2016;33(7):1870-4.
30. Flot JF. SeqPHASE: a web tool for interconverting PHASE input/output files and FASTA sequence alignments. Molecular Ecology Resources. 2010;10(1):162-6.

31. Stephens M, Donnelly P. A comparison of bayesian methods for haplotype reconstruction from population genotype data. The American Journal of Human Genetics. 2003;73(5):1162-9.
32. Stephens M, Smith NJ, Donnelly P. A new statistical method for haplotype reconstruction from population data. The American Journal of Human Genetics. 2001;68(4):978-89.
33. Kearse M, Moir R, Wilson A, Stones-Havas S, Cheung M, Sturrock S, et al. Geneious Basic: An integrated and extendable desktop software platform for the organization and analysis of sequence data. Bioinformatics. 2012;28(12):1647-9.
34. Van Oosterhout C, Hutchinson WF, Wills DPM, Shipley P. MICRO-CHECKER: Software for identifying and correcting genotyping errors in microsatellite data. Molecular Ecology Notes. 2004;4(3):535-8.
35. Rousset F. GENEPOP'007: a complete re-implementation of the GENEPOP software for Windows and Linux. Molecular Ecology Resources. 2008;8(1):103-6.
36. Rice WR. Analyzing tables of statistical tests. Evolution. 1989;43(1):223-5.
37. Peakall R, Smouse P. GenAlEx 6.5: Genetic analysis in Excel. Population genetic software for teaching and research-an update. Bioinformatics. 2012;28(19):2537-9.
38. Kalinowski ST. hp-rare 1.0: a computer program for performing rarefaction on measures of allelic richness. Molecular Ecology Notes. 2005;5(1):187-9.
39. Belkhir K, Borsa P, Chikhi L, Raufaste N, Bonhomme F. GENETIX 4.05, logiciel sous Windows TM pour la génétique des populations. Laboratoire Génome, Populations, Interactions, CNRS UMR 5000, Université de Montpellier II, Montpellier (France). 1996-2004.
40. Salzburger W, Ewing GB, Von Haeseler A. The performance of phylogenetic algorithms in estimating haplotype genealogies with migration. Molecular Ecology. 2011;20(9):1952-63.
41. Darriba D, Taboada GL, Doallo R, Posada D. jModelTest 2: More models, new heuristics and parallel computing. Nature Methods. 2012;9(8):772.
42. Stamatakis A. RAxML-VI-HPC: maximum likelihood-based phylogenetic analyses with thousands of taxa and mixed models. Bioinformatics. 2006;22(21):2688-90.
43. Rozas J, Ferrer-Mata A, Sánchez-DelBarrio JC, Guirao-Rico S, Librado P, Ramos-Onsins SE, et al. DnaSP 6: DNA sequence polymorphism analysis of large data sets. Molecular Biology and Evolution. 2017;34(12):3299-302.
44. Heled J, Drummond AJ. Bayesian inference of species trees from multilocus data. Molecular Biology and Evolution. 2009;27(3):570-80.
45. Drummond AJ, Rambaut A. BEAST: Bayesian evolutionary analysis by sampling trees. BMC Evolutionary Biology. 2007;7(1):1-8.
46. Jombart T, Devillard S, Balloux F. Discriminant analysis of principal components: A new method for the analysis of genetically structured populations. BMC Genetics. 2010;11(1):94.
47. R Core Team. R: A language and environment for statistical computing. Vienna, Austria: R Foundation for Statistical Computing. http://www.R-project.org/. 2018.
48. Pritchard JK, Stephens M, Donnelly P. Inference of population structure using multilocus genotype data. Genetics. 2000;155(2):945-59.

873 49. Takezaki N, Nei M, Tamura K. POPTREEW: web version of POPTREE for constructing
874 population trees from allele frequency data and computing some other quantities.
875 Molecular Biology and Evolution. 2014;31(6):1622-4.
876 50. Caye K, Jay F, Michel O, François O. Fast inference of individual admixture
877 coefficients using geographic data. The Annals of Applied Statistics. 2018;12(1):586-
878 608.
879 51. Excoffier L, Lischer HE. Arlequin suite ver 3.5: a new series of programs to perform
880 population genetics analyses under Linux and Windows. Molecular Ecology
881 Resources. 2010;10(3):564-7.
882 52. Excoffier L, Smouse PE, Quattro JM. Analysis of molecular variance inferred from
883 metric distances among DNA haplotypes: Application to human mitochondrial DNA
884 restriction data. Genetics. 1992;131(2):479-91.
885 53. Dufresnes C, Litvinchuk SN, Leuenberger J, Ghali K, Zinenko O, Stöck M, et al.
886 Evolutionary melting pots: a biodiversity hotspot shaped by ring diversifications
887 around the Black Sea in the Eastern tree frog (*Hyla orientalis*). Molecular Ecology.
888 2016;25(17):4285-300.
889 54. Jones OR, Wang J. COLONY: A program for parentage and sibship inference from
890 multilocus genotype data. Molecular Ecology Resources. 2010;10(3):551-5.
891 55. Lucati F, Poignet M, Miró A, Trochet A, Aubret F, Barthe L, et al. Multiple glacial
892 refugia and contemporary dispersal shape the genetic structure of an endemic
893 amphibian from the Pyrenees. Molecular Ecology. 2020;29(15):2904-21.
894 56. Cornuet JM, Pudlo P, Veyssier J, Dehne-Garcia A, Gautier M, Leblois R, et al. DIYABC
895 v2.0: A software to make approximate Bayesian computation inferences about
896 population history using single nucleotide polymorphism, DNA sequence and
897 microsatellite data. Bioinformatics. 2014;30(8):1187-9.
898 57. Emerson BC, Hewitt GM. Phylogeography. Current Biology. 2005;15(10):R367-R71.
899 58. Chamorro D, Martínez-Freiría F, Real R, Muñoz AR. Understanding parapatry: How do
900 environment and competitive interactions shape Iberian vipers' distributions?
901 Journal of Biogeography. 2020.
902 59. Martínez-Freiría F, Freitas I, Zuffi MA, Golay P, Ursenbacher S, Velo-Antón G. Climatic
903 refugia boosted allopatric diversification in western Mediterranean vipers. Journal of
904 Biogeography. 2020;47(8):1698-713.
905 60. Antunes B, Velo-Antón G, Buckley D, Pereira R, Martínez-Solano I. Physical and
906 ecological isolation contribute to maintain genetic differentiation between fire
907 salamander subspecies. Heredity. 2021:1-14.
908 61. Dufresnes C, Pribille M, Alard B, Gonçalves H, Amat F, Crochet P-A, et al. Integrating
909 hybrid zone analyses in species delimitation: Lessons from two anuran radiations of
910 the Western Mediterranean. Heredity. 2020;124(3):423-38.
911 62. Sánchez-Montes G, Wang J, Ariño AH, Martínez-Solano Í. Mountains as barriers to
912 gene flow in amphibians: Quantifying the differential effect of a major mountain
913 ridge on the genetic structure of four sympatric species with different life history
914 traits. Journal of Biogeography. 2018;45(2):318-31.
915 63. Li Y, Zhang X, Fang Y. Landscape features and climatic forces shape the genetic
916 structure and evolutionary history of an oak species (*Quercus chenii*) in East China.
917 Frontiers in Plant Science. 2019;10:1060.

64. Wallis GP, Waters JM, Upton P, Craw D. Transverse alpine speciation driven by glaciation. Trends in Ecology & Evolution. 2016;31(12):916-26.
65. Alcaide M, Scordato ES, Price TD, Irwin DE. Genomic divergence in a ring species complex. Nature. 2014;511(7507):83-5.
66. Irwin D, Wake D. Ring species. In: Kliman RM, editor. Encyclopedia of evolutionary biology. 3. Oxford: Academic Press; 2016. p. 467–75.
67. Monahan WB, Pereira RJ, Wake DB. Ring distributions leading to species formation: a global topographic analysis of geographic barriers associated with ring species. BMC Biology. 2012;10(1):1-15.
68. Irwin DE, Irwin JH, Price TD. Ring species as bridges between microevolution and speciation. Genetica. 2001;112-113:223-43.
69. Kuchta SR, Wake DB. Wherefore and whither the ring species? 2016;104(1):189-201.
70. Bouzid NM, Archie JW, Anderson RA, Grummer JA, Leaché AD. Evidence for ephemeral ring species formation during the diversification history of western fence lizards (*Sceloporus occidentalis*). Molecular Ecology. 2021.
71. Alley RB, Mayewski PA, Sowers T, Stuiver M, Taylor KC, Clark PU. Holocene climatic instability: A prominent, widespread event 8200 yr ago. Geology. 1997;25(6):483-6.
72. Bidegaray-Batista L, Sánchez-Gracia A, Santulli G, Maiorano L, Guisan A, Vogler AP, et al. Imprints of multiple glacial refugia in the Pyrenees revealed by phylogeography and palaeodistribution modelling of an endemic spider. Molecular Ecology. 2016;25(9):2046-64.
73. Charrier O, Dupont P, Pornon A, Escaravage N. Microsatellite marker analysis reveals the complex phylogeographic history of *Rhododendron ferrugineum* (Ericaceae) in the Pyrenees. PLoS One. 2014;9(3):e92976.
74. Liberal IM, Burrus M, Suchet C, Thebaud C, Vargas P. The evolutionary history of *Antirrhinum* in the Pyrenees inferred from phylogeographic analyses. BMC Evolutionary Biology. 2014;14(1):146.
75. Donaire-Barroso D, Rivera X. La salamandra común *Salamandra salamandra* (Linnaeus, 1758) en el subcantábrico: Origen, dispersión, subespecies y zonas de introgresión. Butlletí Societat Catalana de Herpetología. 2016;23:7-38.
76. Thielsch A, Knell A, Mohammadyari A, Petrusek A, Schwenk K. Divergent clades or cryptic species? Mito-nuclear discordance in a *Daphnia* species complex. BMC Evolutionary Biology. 2017;17(1):227.
77. Díaz-Rodríguez J, Gehara M, Marquez R, Vences M, Goncalves H, Sequeira F, et al. Integration of molecular, bioacoustical and morphological data reveals two new cryptic species of *Pelodytes* (Anura, Pelodytidae) from the Iberian Peninsula. Zootaxa. 2017;4243(1):1-41.
78. Díaz-Rodríguez J, Gonçalves H, Sequeira F, Sousa-Neves T, Tejedo M, Ferrand N, et al. Molecular evidence for cryptic candidate species in Iberian *Pelodytes* (Anura, Pelodytidae). Molecular Phylogenetics and Evolution. 2015;83:224-41.
79. Barbosa S, Pauperio J, Herman JS, Ferreira CM, Pita R, Vale-Goncalves HM, et al. Endemic species may have complex histories: within-refugium phylogeography of an endangered Iberian vole. Molecular Ecology. 2017;26(3):951-67.

80. Noguerales V, Cordero PJ, Ortego J. Inferring the demographic history of an oligophagous grasshopper: Effects of climatic niche stability and host-plant distribution. Mol Phylogenet Evol. 2018;118:343-56.
81. Canestrelli D, Bisconti R, Sacco F, Nascetti G. What triggers the rising of an intraspecific biodiversity hotspot? Hints from the agile frog. Scientific Reports. 2014;4:5042.
82. Dufresnes C, Nicieza AG, Litvinchuk SN, Rodrigues N, Jeffries DL, Vences M, et al. Are glacial refugia hotspots of speciation and cyto-nuclear discordances? Answers from the genomic phylogeography of Spanish common frogs. Molecular Ecology. 2020;29:986-1000.
83. Domènech M, Crespo LC, Enguídanos A, Arnedo MA. Mitochondrial discordance in closely related *Theridion* spiders (Araneae, Theridiidae), with description of a new species of the *T. melanurum* group. Zoosystematics Evolution. 2020;96:159.
84. Escoda L, Castresana J. The genome of the Pyrenean desman and the effects of bottlenecks and inbreeding on the genomic landscape of an endangered species. Evolutionary Applications. 2021.
85. Recuero E, Garcia-Paris M. Evolutionary history of *Lissotriton helveticus*: Multilocus assessment of ancestral vs. recent colonization of the Iberian Peninsula. Molecular Phylogenetics and Evolution. 2011;60(1):170-82.
86. Irwin DE. Phylogeographic breaks without geographic barriers to gene flow. Evolution. 2002;56(12):2383-94.
87. Godet C, Clauzel C. Comparison of landscape graph modelling methods for analysing pond network connectivity. Landscape Ecology. 2021;36(3):735-48.
88. O'Hanlon SJ, Rieux A, Farrer RA, Rosa GM, Waldman B, Bataille A, et al. Recent Asian origin of chytrid fungi causing global amphibian declines. Science. 2018;360(6389):621-7.
89. Bosch J, Fernández-Beaskoetxea S, Garner TW, Carrascal LM. Long-term monitoring of an amphibian community after a climate change- and infectious disease-driven species extirpation. Global Change Biology. 2018;24(6):2622-32.
90. Bosch J. Sapo partero común (*Alytes obstetricans*). In: Pleguezuelos JM, Márquez R, Lizana M, editors. Atlas y libro rojo de los anfibios y reptiles de España. Madrid, Spain: Dirección General de Conservación de la Naturaleza-Asociación Herpetologica Española; 2002. p. 82–4.
91. McKnight DT, Schwarzkopf L, Alford RA, Bower DS, Zenger KR. Effects of emerging infectious diseases on host population genetics: a review. Conservation Genetics. 2017;18(6):1235-45.
92. Cornuet JM, Ravigne V, Estoup A. Inference on population history and model checking using DNA sequence and microsatellite data with the software DIYABC (v1.0). BMC Bioinformatics. 2010;11:401.
93. Cabrera AA, Palsbøll PJ. Inferring past demographic changes from contemporary genetic data: A simulation-based evaluation of the ABC methods implemented in DIYABC. Molecular Ecology Resources. 2017;17(6):e94-e110.
94. Ebdon S, Laetsch DR, Dapporto L, Hayward A, Ritchie MG, Dincă V, et al. The Pleistocene species pump past its prime: Evidence from European butterfly sister species. bioRxiv. 2021.

95. Vences M, Hauswaldt JS, Steinfartz S, Rupp O, Goesmann A, Künzel S, et al. Radically different phylogeographies and patterns of genetic variation in two European brown frogs, genus *Rana*. Molecular Phylogenetics and Evolution. 2013;68(3):657-70.
96. Vences M, Sarasola-Puente V, Sanchez E, Amat F, Hauswaldt JS. Diversity and distribution of deep mitochondrial lineages of the common frog, *Rana temporaria*, in northern Spain. Salamandra. 2017;53:25-33.
97. Uy JAC, Borgia G. Sexual selection drives rapid divergence in bowerbird display traits. Evolution. 2000;54(1):273-8.
98. Polo-Cavia N, Oliveira JM, Villa AJR, Márquez R. Background colour matching in a wild population of *Alytes obstetricans*. Amphibia-Reptilia. 2016;37(3):253-60.
99. Evanno G, Regnaut S, Goudet J. Detecting the number of clusters of individuals using the software STRUCTURE: A simulation study. Molecular Ecology. 2005;14(8):2611-20.

Supporting information

S1 Fig. Summary of *A. obstetricans/almogavarii* samples incorporated into each main analysis. (a) Geographic location of populations included in each analysis. For population codes see Fig 1. The inset map shows the distribution of the main lineages: orange - ND4 haplogroups E-F (*A. almogavarii*), yellow - ND4 haplogroup B (*A. o. obstetricans*), blue - ND4 haplogroup A (*A. o. pertinax*), red - ND4 haplogroup C (*A. o. boscai*), green - ND4 haplogroup D (*A. o. boscai*), black - unclear (adapted from Dufresnes and Martínez-Solano [23]). (b) Markers used in each analysis, with the corresponding number of samples and populations. Effective population sizes were calculated only for populations with ≥ 15 genotyped individuals. In the case of demographic history, only high mountain populations were included in the analysis.

S2 Fig. Results of phylogenetic and clustering analyses for *Alytes obstetricans/almogavarii*. (a) Geographic distribution of the four mtDNA (ND4) haplogroups recovered in the analysis (blue: mtDNA haplogroup A, yellow: mtDNA haplogroup B, grey: mtDNA haplogroup E, orange: mtDNA haplogroup F). In four populations (T2, 61XR, BP and PI) we detected the presence of more than one haplogroup. (b) Results from Discriminant Analysis of Principal Components (DAPC) and (c) STRUCTURE for K = 7 microsatellite groups (see Fig 4). (d) Geographic distribution of the five genetic groups identified by microsatellite-based neighbour-

joining analysis (see S7 Fig). White circles indicate populations with no data available for either ND4 or microsatellites. For population codes see Fig 1. The inset map shows the distribution of the main lineages: orange - ND4 haplogroups E-F (*A. almogavarii*), yellow - ND4 haplogroup B (*A. o. obstetricans*), blue - ND4 haplogroup A (*A. o. pertinax*), red - ND4 haplogroup C (*A. o. boscai*), green - ND4 haplogroup D (*A. o. boscai*), black - unclear (adapted from Dufresnes and Martínez-Solano [23]).

S3 Fig. *Alytes* species tree produced in *BEAST based on one nuclear gene (β-fibint7) and four mitochondrial fragments (ND4, cyt-*b*, 12S and 16S). Labels on branch tips correspond to the distinct ND4 haplogroups identified (blue: mtDNA haplogroup A, pink: mtDNA haplogroup B (central-western Pyrenean populations), yellow: mtDNA haplogroup B (Picos de Europa populations), grey: mtDNA haplogroup E, orange: mtDNA haplogroup F). Posterior probabilities of lineage divergence are indicated on branch labels.

S4 Fig. Resulting plots from Discriminant Analysis of Principal Components (DAPC) across all *Alytes obstetricans/almogavarii* populations. (a) Summary plots for K = 2-7 genetic clusters. At K = 2, genetic clusters are represented as density curves. At K = 3-7, dots represent individuals and genetic clusters are shown as inertia ellipses. Legend labels indicate the different genetic clusters: eastern Pyrenees (EPY, orange), central Pyrenees (CPY, grey), central-western Pyrenees (CWPY, pink), Picos de Europa

mountains (PEU, yellow), and Guadarrama Mountain Range (GUA, blue). (b) Distribution of BIC (Bayesian Information Criterion) values according to the number of clusters. The red arrow indicates the number of clusters chosen for DAPC analysis. The optimal number of clusters was assessed using the *find.clusters* function and determined as the K value above which BIC (Bayesian Information Criterion) values decreased substantially.

S5 Fig. Results of Bayesian clustering analyses in STRUCTURE for microsatellites. (a) Mean (± SD) log probability of the data [Ln Pr(XIK)] over 10 runs, for each value of K. (b) ΔK values as a function of K, calculated according to Evanno et al. [99].

S6 Fig. Results of Tess3R analyses for microsatellites. (a) Map depicting the distribution of ancestry coefficients inferred through Tess3R for K = 7 clusters. Black dots indicate the populations analysed. Colour codes as for STRUCTURE results. More saturated colours indicate a greater proportion of ancestry to either cluster. (b) Distribution of cross-validation scores according to the number of clusters. The red arrow indicates the number of clusters chosen for Tess3R analysis.

S7 Fig. Neighbour-joining tree based on D_A distances for microsatellite markers. Branch colours delineate the seven genetic clusters inferred by STRUCTURE (see Figs 4a and 5), while colour shades around population codes correspond to the distinct

mtDNA (ND4) haplogroups (blue: mtDNA haplogroup A, yellow: mtDNA haplogroup B, grey: mtDNA haplogroup E, orange: mtDNA haplogroup F; see Fig 3). In four populations (T2, 61XR, BP and PI) we detected the presence of more than one haplogroup. For population codes see S1 Table.

S1 Table. Geographic information and standard genetic statistics of *Alytes obstetricans/almogavarii* sampling localities. Populations are grouped according to the genetic group of interest (EPY: eastern Pyrenees, CPY: central Pyrenees, CWPY: central-western Pyrenees, PEU: Picos de Europa mountains, GUA: Guadarrama Mountain Range). Lat. – latitude, Long. – longitude, Alt. – altitude in meters, N – sample size for microsatellites, Na – mean number of alleles, Ar – allelic richness standardized for sample size, H_O – observed heterozygosity, H_E – expected heterozygosity, F_{IS} – inbreeding coefficient, N_e – effective population size, N ND4 – sample size for ND4, ND4 haps – occurrence and code (in parentheses) of mitochondrial ND4 haplogroups identified in each population (see Fig 3), N cyt-b – sample size for cyt-*b*, N 12S – sample size for 12S, N 16S – sample size for 16S, N β-fibint7 – sample size for β-fibint7.

S2 Table. Parameters used in DIYABC analysis and respective priors for the best supported scenarios. The best supported scenarios were scenario 2 when considering only microsatellites (simple sequence repeats – SSRs) and scenario 5

when including both mtDNA (ND4) and microsatellite markers. See Fig 2 for more information on tested scenarios. N – effective population size for each analysed deme (EPY – eastern Pyrenees; CPY – central Pyrenees; CWPY – central-western Pyrenees; PEU – Picos de Europa Mountains, GUA – Guadarrama Mountains), ra – admixture rate, t – time of events in generations (t_1 – time to the most recent split; t_2 – time to the intermediate split; t_3 – time to the most ancient split). Microsatellite (SSRs) and mitochondrial (ND4) parameters: mean μ – mean mutation rate, individual locus μ – individual locus mutation rate, mean *P* – mean coefficient *P*, individual locus *P* – individual locus coefficient *P*, SNI – Single Nucleotide Insertion rate, mean *k* – mean coefficient *k*, individual locus *k* – individual locus coefficient *k*. Microsatellite loci were divided in two groups depending on the motif length (tri- and tetranucleotide loci). Conditions: sequence data were simulated under a Tamura Nei (TN93) mutation model.

S3 Table. Microsatellite-based (below diagonal) and ND4-based (above diagonal) pairwise estimates of F_{ST} between the seven genetic groups identified by STRUCTURE in *Alytes obstetricans/almogavarii* (see Fig 5). All P values < 0.01.

S4 Table. Analysis of molecular variance (AMOVA) for mitochondrial (ND4) and nuclear (microsatellites) markers based on the seven genetic groups identified by STRUCTURE in *Alytes obstetricans/almogavarii* (see Fig 5). All P values < 0.001.

S5 Table. Posterior probability of tested scenarios and 95% confidence intervals (CI) estimated with DIYABC analysis when considering only microsatellites and when including both mtDNA (ND4) and microsatellite markers. Type I and II errors for the best supported scenarios are indicated. See Fig 2 for more information on tested scenarios.

S6 Table. Posterior parameters (median and 95% confidence intervals) and RMedAD (Relative Median Absolute Deviation) estimated with DIYABC analysis for the best supported scenarios when considering only microsatellites (simple sequence repeats – SSRs; scenario 2) and when including both mtDNA (ND4) and microsatellite markers (scenario 5). See Fig 2 for more information on tested scenarios. N – effective population size for each analysed deme (EPY – eastern Pyrenees; CPY – central Pyrenees; CWPY – central-western Pyrenees; PEU – Picos de Europa Mountains; GUA – Guadarrama Mountains), ra – admixture rate, t – time of events in generations (t_1 – time to the most recent split; t_2 – time to the intermediate split; t_3 – time to the most ancient split), mean μ – mean mutation rate, mean *P* – mean coefficient *P*, mean *k* – mean coefficient *k*, $Q_{2.5}$ – quantile 2.5%, $Q_{97.5}$ – quantile 97.5%.

S1 Appendix. Supporting methods.

Figure

Click here to access/download;Figure;Figuresnewnew.docx

Fig 1

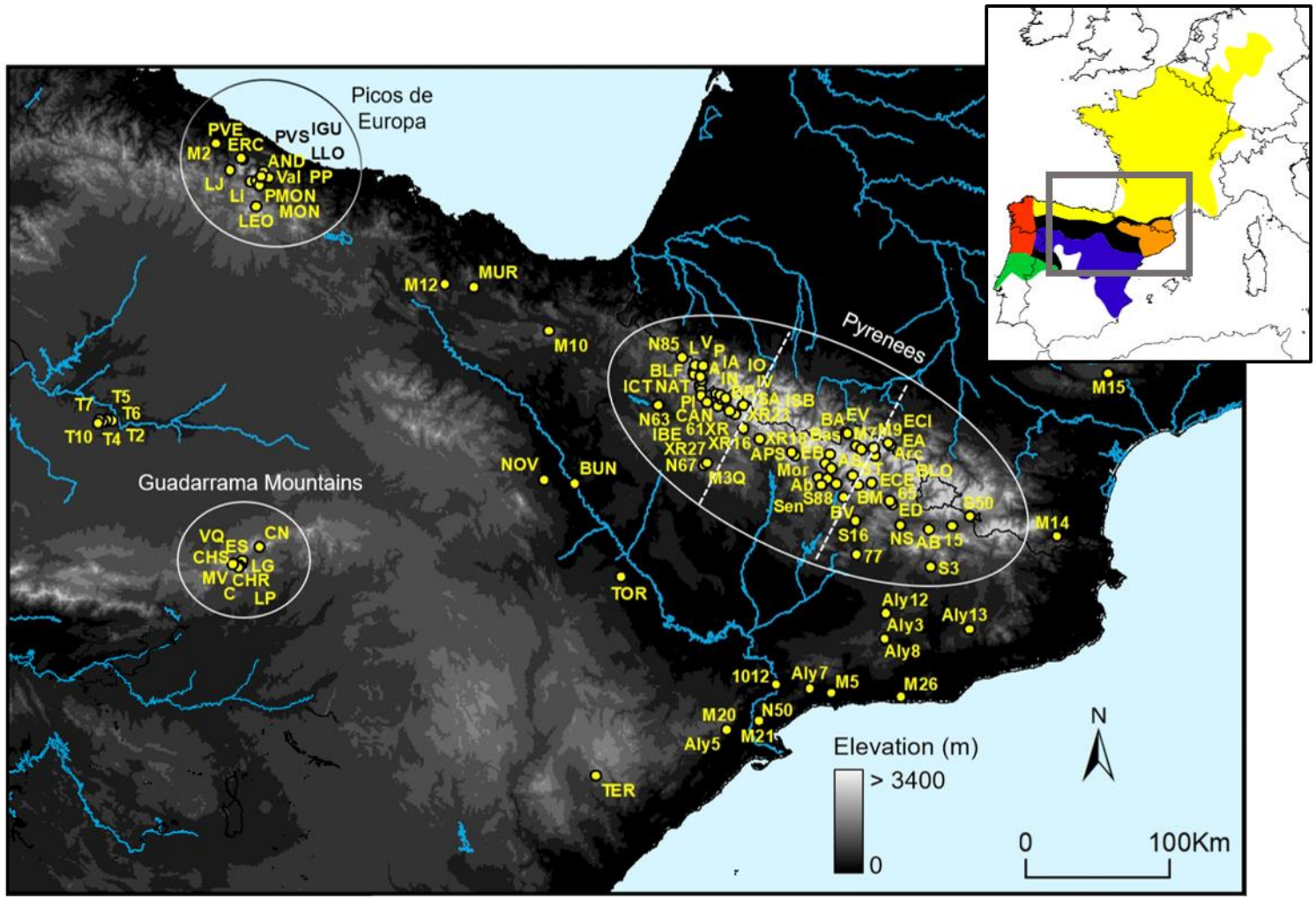

Fig 2

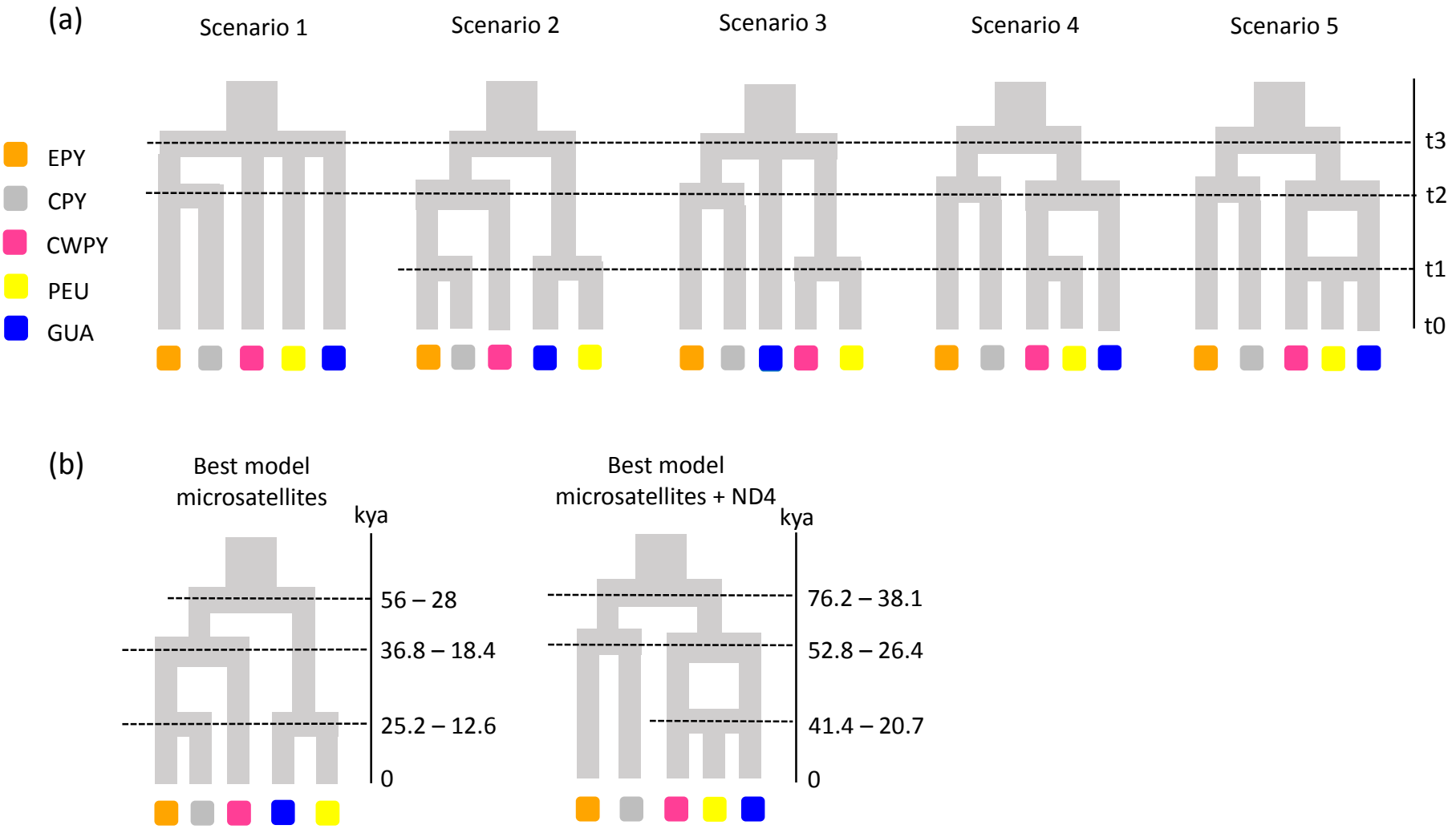
(a)
Scenario 1
Scenario 2
Scenario 3
Scenario 4
Scenario 5
EPY
CPY
CWPY
PEU
GUA
t3
t2
t1
t0
(b)
Best model microsatellites
kya
56 – 28
36.8 – 18.4
25.2 – 12.6
0
Best model microsatellites + ND4
kya
76.2 – 38.1
52.8 – 26.4
41.4 – 20.7
0

Fig 3

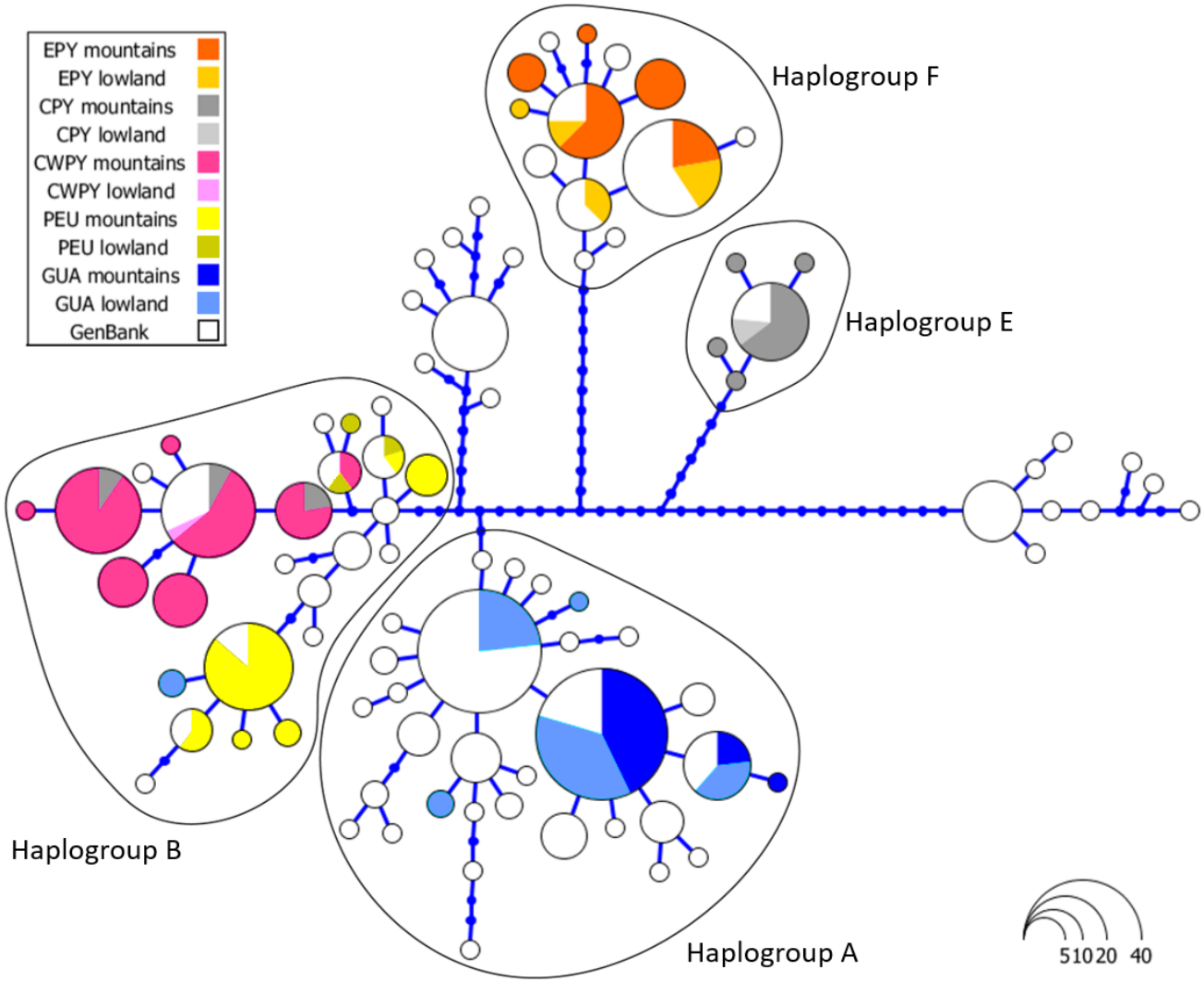
EPY mountains
EPY lowland
CPY mountains
CPY lowland
CWPY mountains
CWPY lowland
PEU mountains
PEU lowland
GUA mountains
GUA lowland
GenBank
Haplogroup F
Haplogroup E
Haplogroup B
Haplogroup A
5 10 20 40

Fig 4

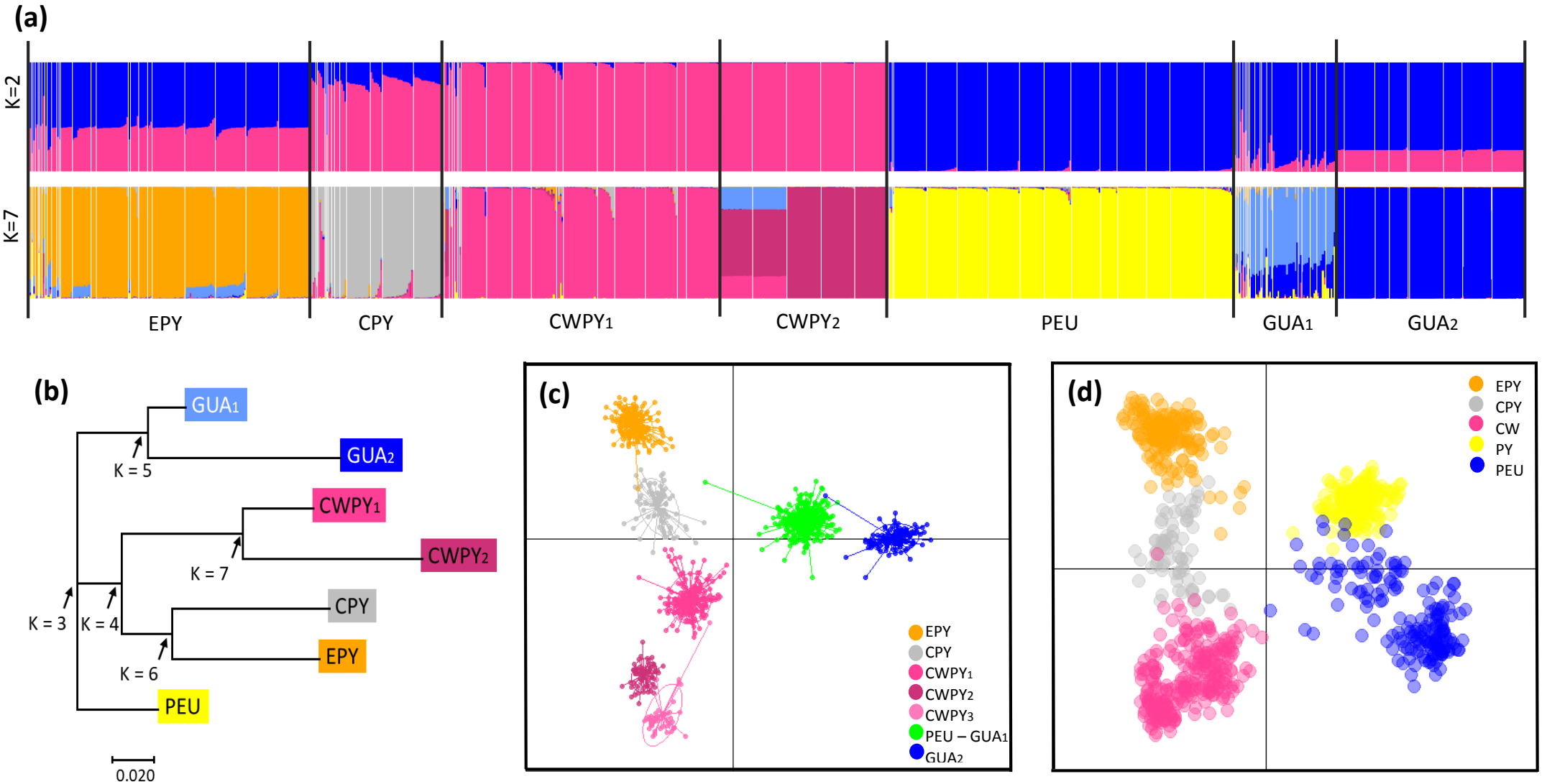
(a)
K=2
K=7
EPY
CPY
CWPY1
CWPY2
PEU
GUA1
GUA2
(b)
GUA1
GUA2
K = 5
CWPY1
CWPY2
K = 7
K = 3
K = 4
CPY
EPY
K = 6
PEU
0.020
(c)
EPY
CPY
CWPY1
CWPY2
CWPY3
PEU – GUA1
GUA2
(d)
EPY
CPY
CW
PY
PEU

Fig 5

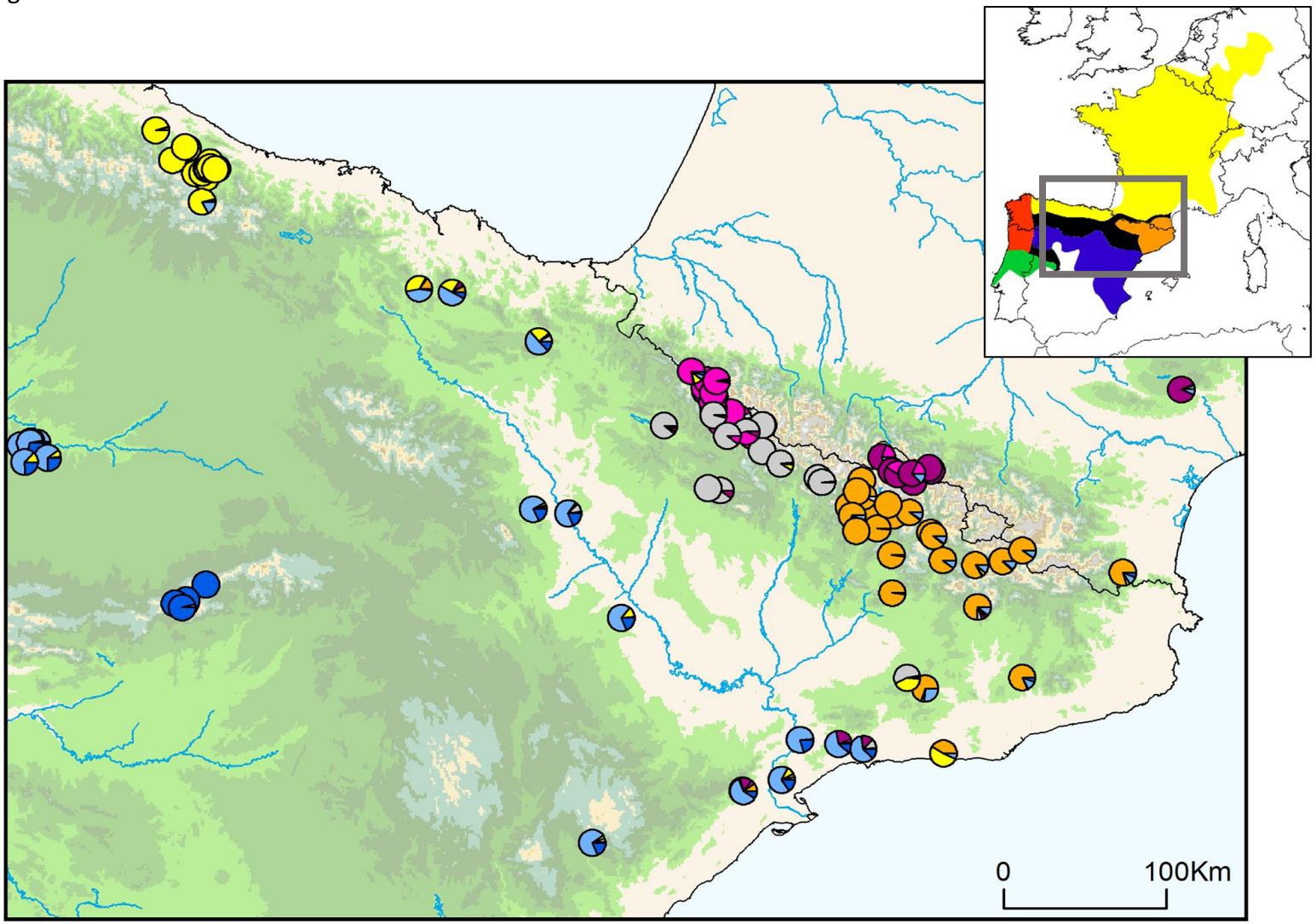

Fig 6

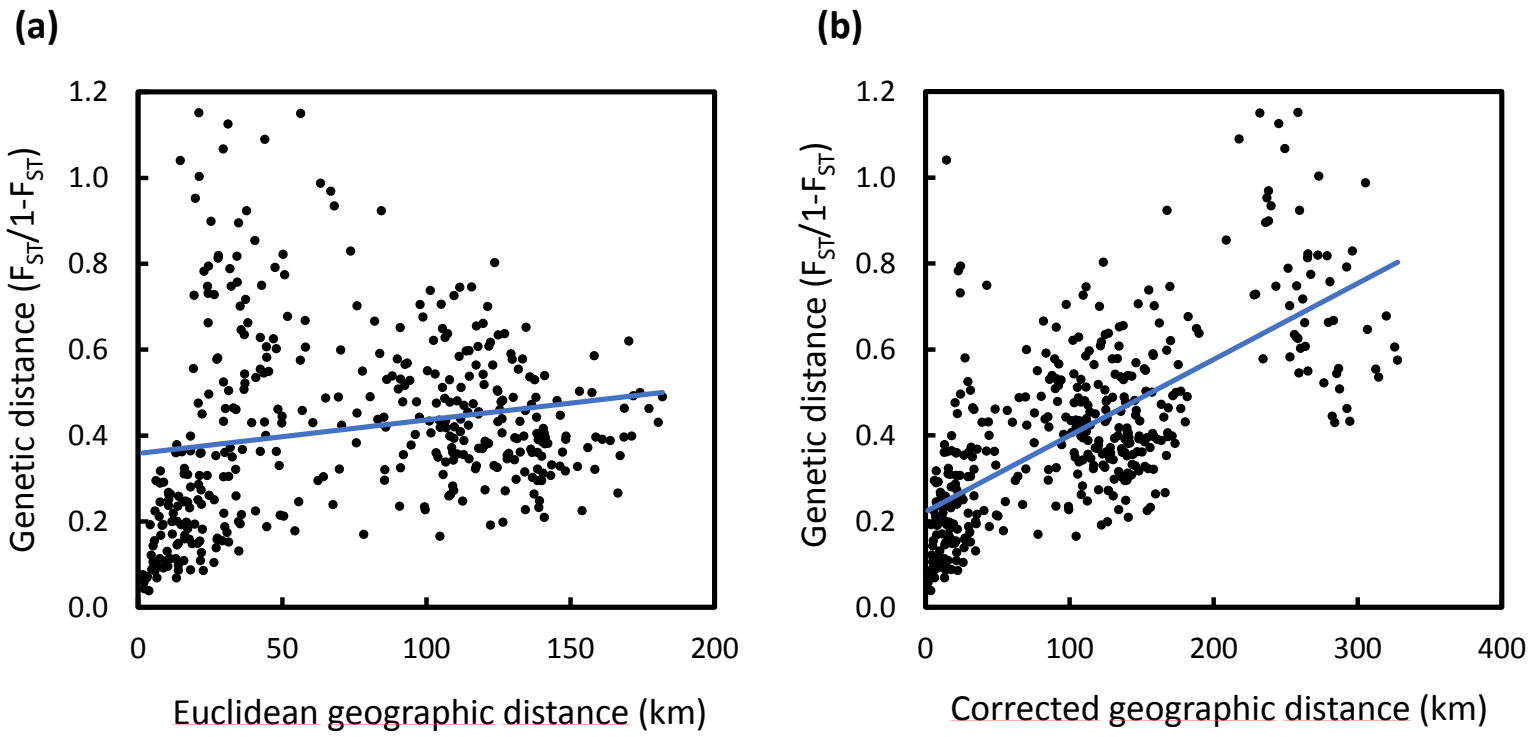
(a)
(b)
Genetic distance (F_{ST}/1-F_{ST})
1.2
1.0
0.8
0.6
0.4
0.2
0.0
0
50
100
150
200
Euclidean geographic distance (km)
Genetic distance (F_{ST}/1-F_{ST})
1.2
1.0
0.8
0.6
0.4
0.2
0.0
0
100
200
300
400
Corrected geographic distance (km)